

High Resolution Mapping of the Unshocked Ejecta in Cassiopeia A

Danielle Dickinson¹, Danny Milisavljević^{1,2}, J. Martin Laming³, Tea Temim⁴, Ilse De Looze⁵, Bon-Chul Koo⁶, John C. Raymond⁷, Richard G. Arendt^{8,9}, Rob Fesen¹⁰, Grace Katz¹

[1] Purdue Univ., [2] Integrative Data Science Institute, [3] Naval Research Laboratory, [4] Princeton Univ., [5] Ghent Univ., [6] Seoul National Univ., [7] Harvard & Smithsonian, [8] NASA/GSFC, [9] CRESST2/UMBC, [10] Dartmouth College



INTRODUCTION

Cassiopeia A (Cas A) is the youngest Galactic Core-Collapse Supernova Remnant (SNR) descended from a partially stripped star and is one of the best examples of a resolved SNR that can be compared to simulations. The interior ejecta of Cas A has yet to be engulfed by the reverse shock and thus has frozen in the vital dynamics of the original Type IIb SN. Among the most important parameters for constraining theoretical predictions of the explosion are the mass and distribution of Fe and other elements that probe the unshocked ejecta (S, O, Si). Here, we present a map of the unshocked ejecta originally presented in Milisavljević et al. 2024 but are showcasing, in detail, 3-Dimensional (3-D) reconstructions of two columns in the interior ejecta.

OBSERVATIONS

We obtained four JWST MIRI/MRS Integral Field Unit (IFU; Gardner et al. 2023) spectra of Cas A, two of which probe Cas A's central region (P2 and P4, see the central mosaic for their positions). These observations were part of a Cycle 1 JWST Program to survey Cas A (Program #1947; PI: D. Milisavljević). We isolate [S IV] 10.511μm (plotted in blue), [Ne II] 12.814μm (plotted in green), and [O IV] 25.89μm (plotted in red) for this study. Cross sections of P4 and P2 are shown in Figures 1 and 2.

We performed a 3rd order polynomial fit as a continuum subtraction for each spaxel across each of the three lines. For the 3-D reconstructions, we cropped each cube by 3 pixels on each side to remove detector artifacts. We convert RA and DEC into velocity space using the scaling factor 0.022" per km/s (Milisavljević & Fesen 2013). We then linearly interpolated the data in the spectral axis to an equivalent (and greater) resolution as the spatial axis for best representation. Using continuum-subtracted, cropped, interpolated cubes and velocities $|v| < 3500$ km/s, we measure the filling factor and reconstruct the interior ejecta in 3-D.

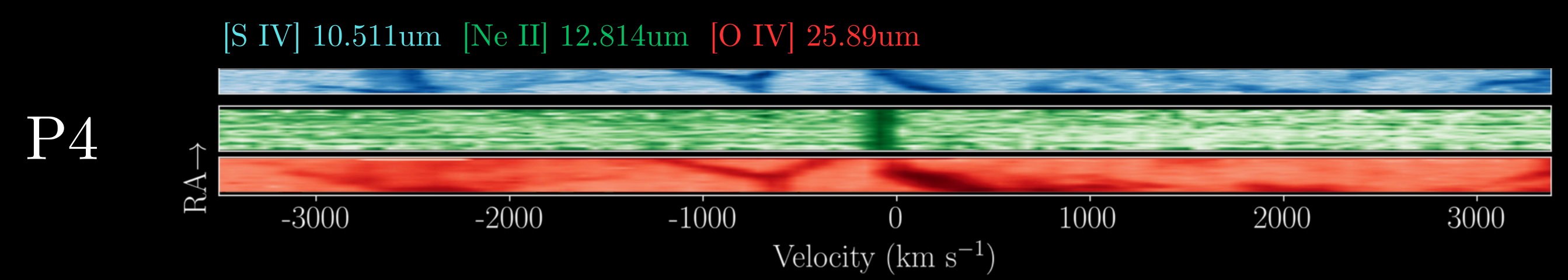


Figure 1: Cross sections of [S IV], [Ne II], and [O IV] in P4. This representation is limited to the velocity range of -3500 to +3500 km/s, but ejecta emission does appear beyond these bounds. We assume all emission $|v| < 3500$ km/s is unshocked ejecta.

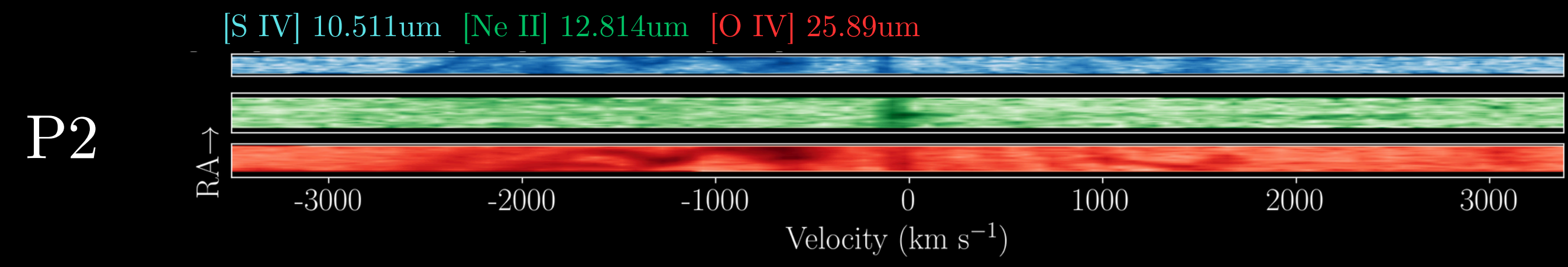


Figure 2: Same as Figure 1 but for P2.



F2550W - F2100W [O IV]
JWST
Courtesy of Judy Schmidt

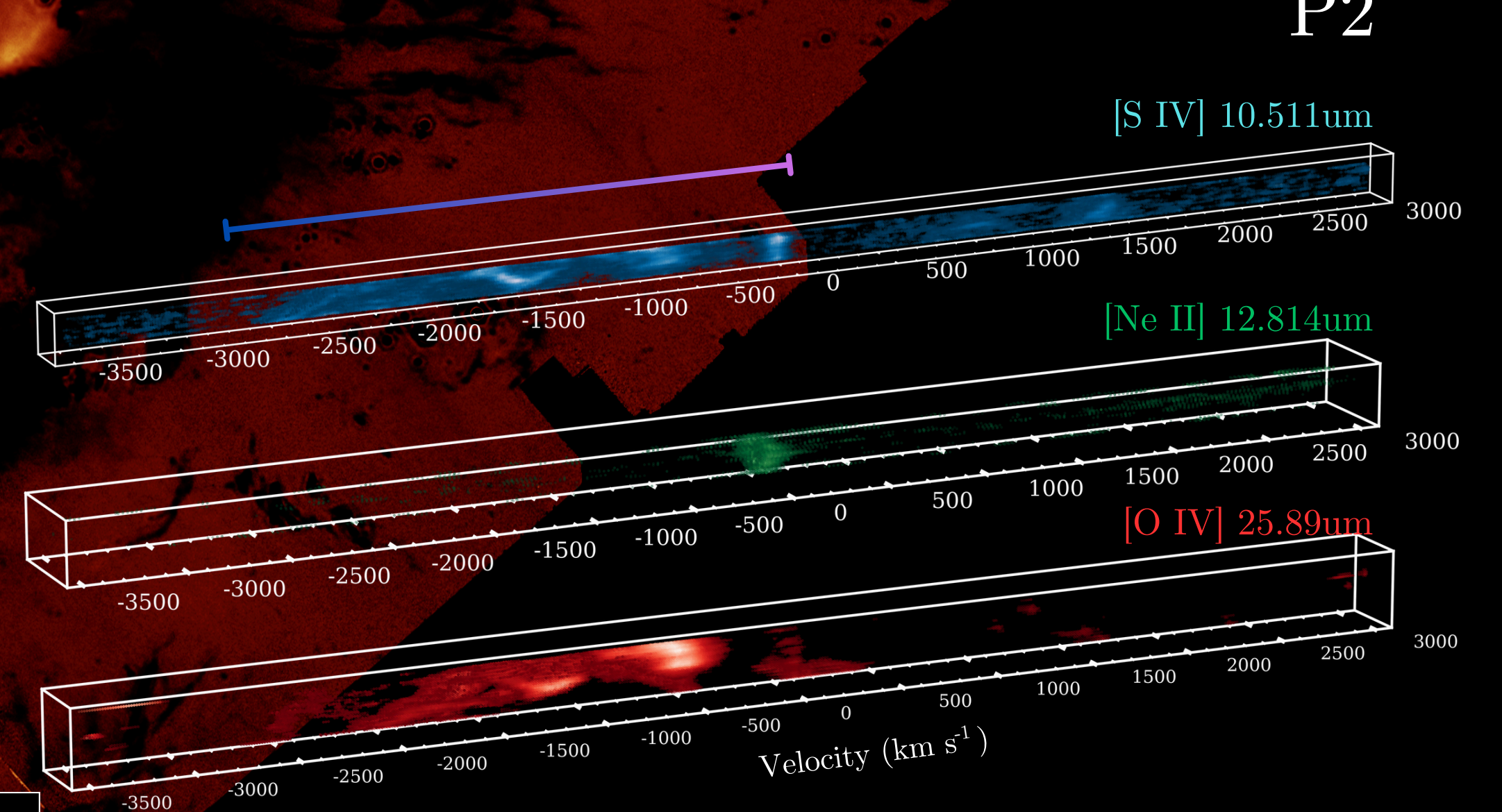
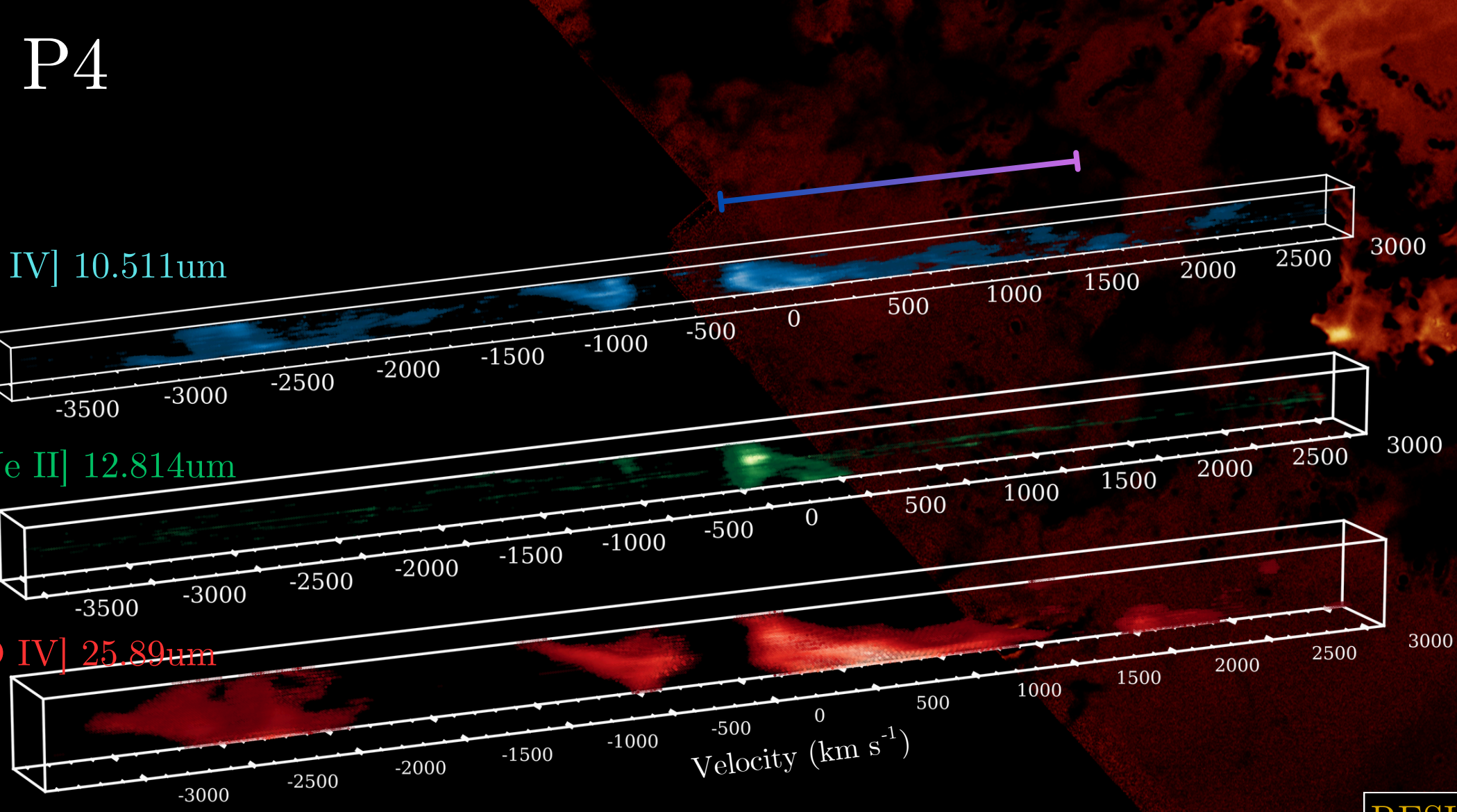
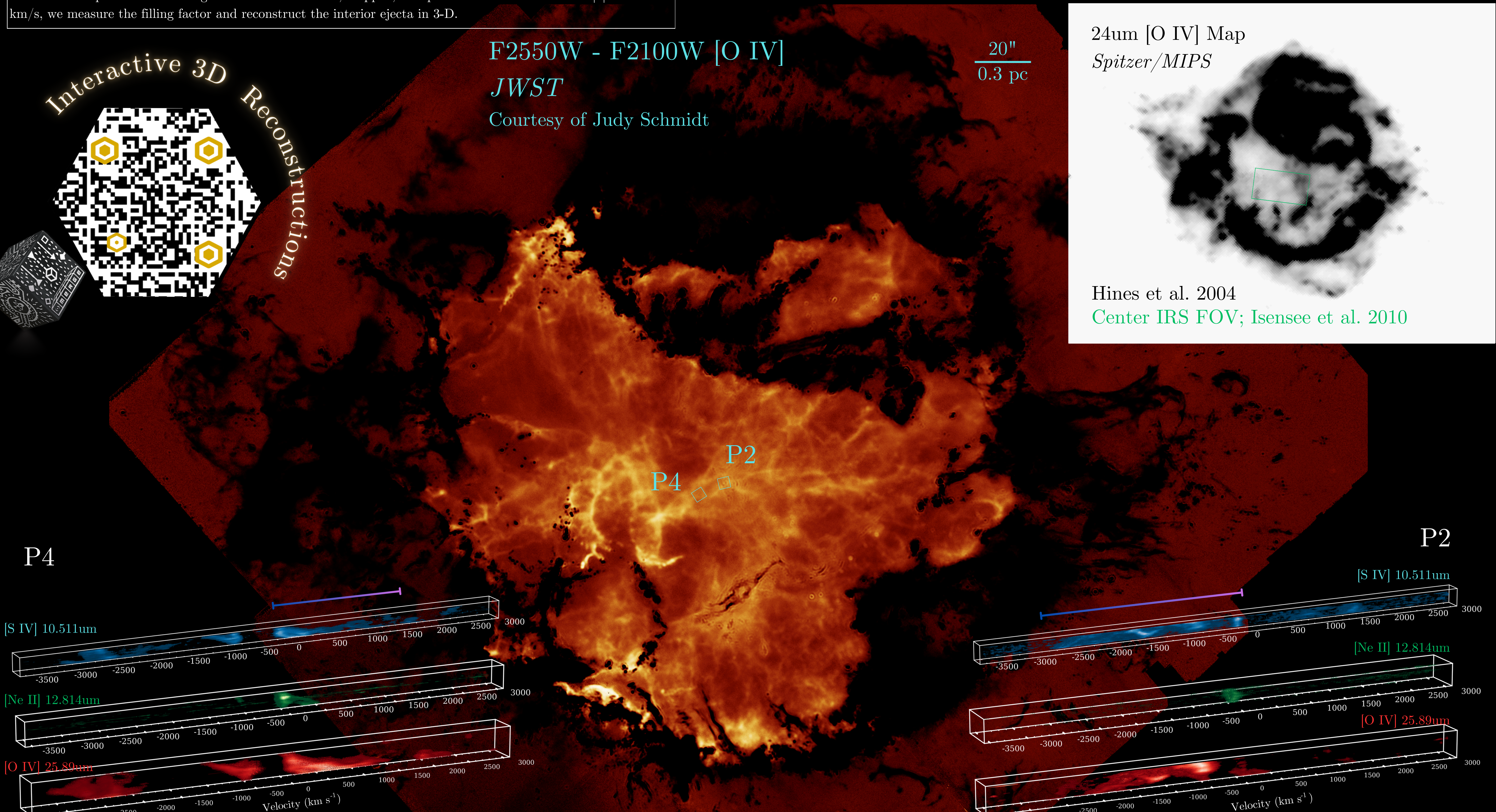
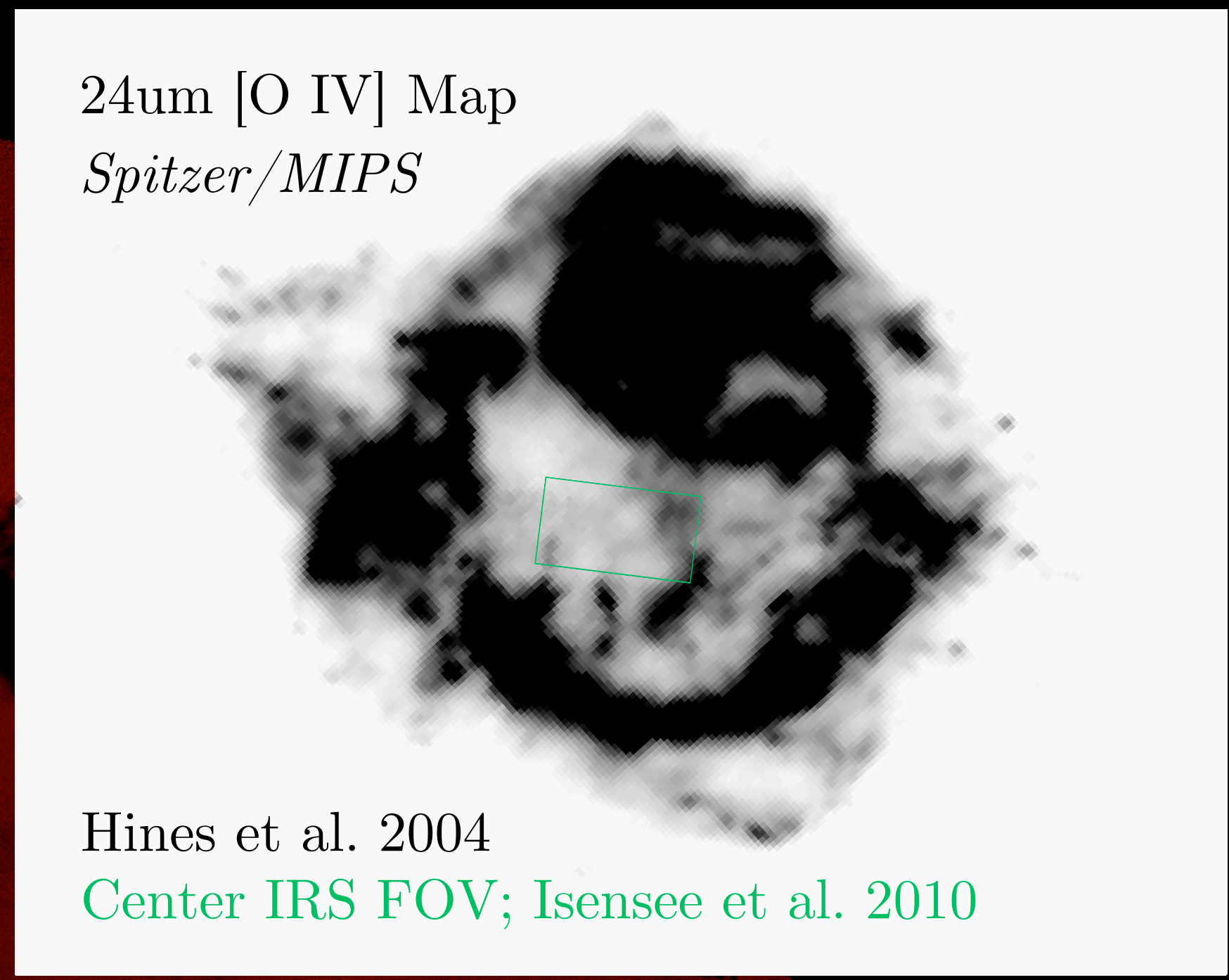


Figure 3: 3-Dimensional reconstructions of [S IV], [Ne II], and [O IV] in P4. Lighter tones indicate higher flux. Data points in [O IV] and [S IV] with fluxes greater than the standard deviation of the background-subtracted cubes are plotted. For [Ne II], data brighter than 3σ is shown.

Figure 4: Same as Figure 3 but for P2.

RESULTS

3-D reconstructions of Cas A's interior ejecta are shown in Figures 3 and 4. All three lines of interest are shown at the full range of velocities for unshocked ejecta. Representations with smaller velocity ranges as well as comparisons to Cas A's main shell (Milisavljević & Fesen 2013) and the central Spitzer IRS data cube (Isensee et al. 2010), whose FOV is the green rectangle in the Spitzer Cas A image, are available on Sketchfab, please scan the hexagonal QR code.

Figures 5 and 6 show narrow band images that step through a selected velocity range in 100 km/s intervals for P4 (-200 to +1300 km/s) and P2 (-2400 to +100 km/s).

We calculate the filling factor for each IFU position and for each ion. While interior ejecta-tracing elements like [O IV] and [S IV] take up about 20% of the volume, [Ne II] takes up 2% of the total volume; in the case of P2, [Ne II] emission is associated with the excitation of circumstellar material in the Green Monster region (De Looze et al. 2024, *in prep*).

DISCUSSION/FUTURE DIRECTION

As seen in the narrow band images and 3-D representations, [S IV] and [O IV] trace each other well. The 3-D reconstructions of these two lines are consistent by the low-resolution *Spitzer* observations in Isensee et al. 2010.

These results will be compared to radiative transfer simulations to accurately constrain the temperatures, densities, and chemical abundances and to improve estimates of the total ejecta mass. Due to the small FOV of the *JWST* IFUs, further observations of other columns must be strategically chosen to accomplish specific science goals. In order to determine the variability in filling factor across Cas A's unshocked ejecta, we suggest randomly choosing > 8 positions spaced $< 1'$ apart throughout the region.

UNSHOCKED IRON

There is weak/candidate Fe emission in the P4 region and implies 0.01 M_{\odot} of unshocked Fe material. However, any potential feature is absent in P2, indicating the Fe is not uniformly distributed. This is an additional motivator for acquiring additional IFU positions with *JWST* across the interior, since Fe traces the original ^{56}Ni distribution.

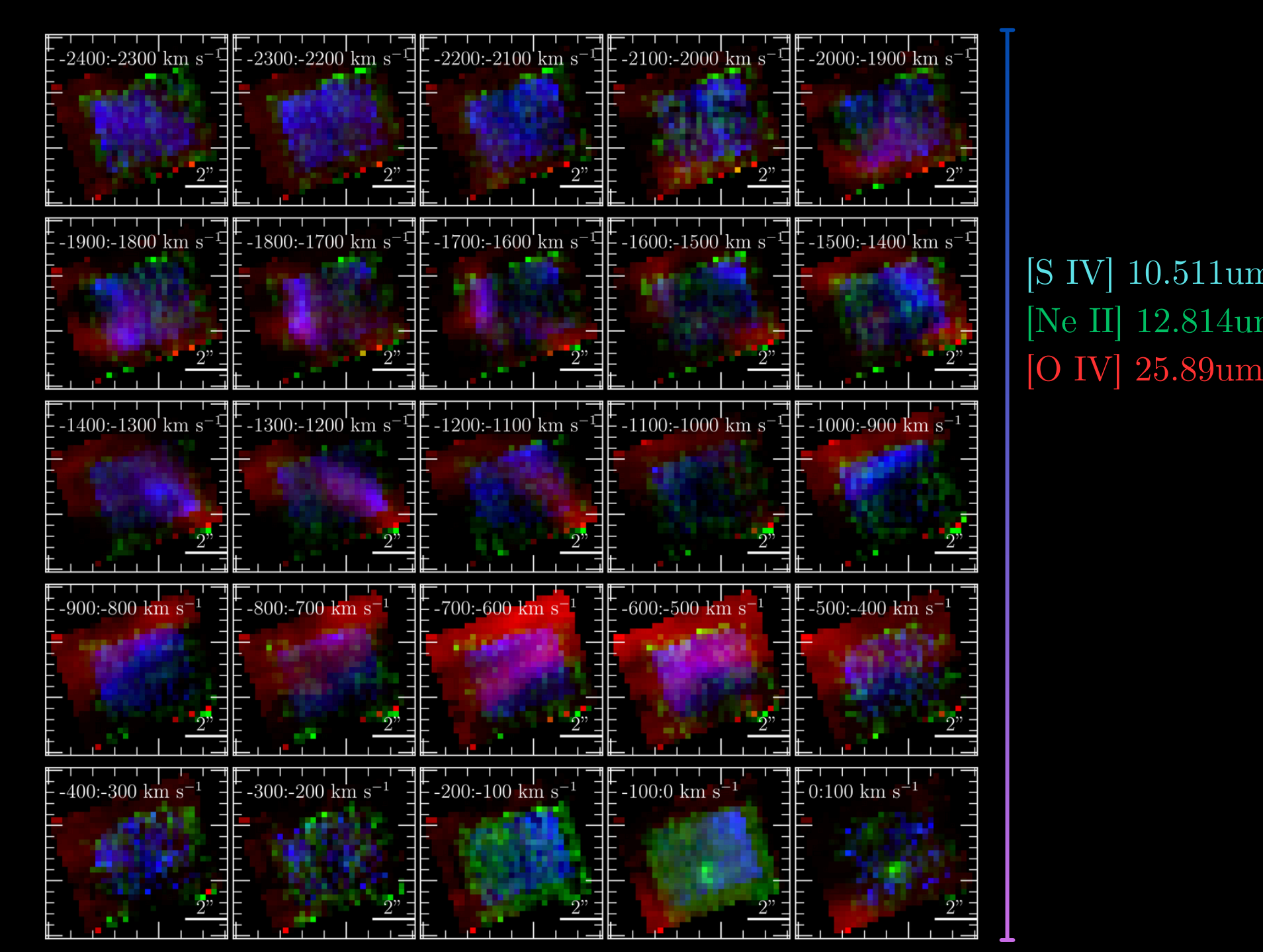


Figure 5: Narrow band imaging of [S IV] (blue), [Ne II] (green), and [O IV] (red) in 100 km/s sections ranging from -200 to +1300 km/s in P4.

Figure 6: Same as Figure 5 but for P2 with the range -2400 to +100 km/s.

CONCLUSIONS

- We observe a web-like network of interior ejecta filaments with scales as small as 0.01pc in two IFU positions in the center of Cas A.
- For [S IV] and [O IV], we measure a filling factor of 19-23% for the interior ejecta.
- These reconstructions are consistent with lower-resolution, archival *Spitzer* observations.
- Additional IFU locations are desirable to probe locations of unshocked Fe and sample a range of filling factors across multiple columns. This will sample potential variation in filling factor and be sensitive to unshocked iron emission.

	10.511μm	12.814μm	25.89μm
P2	0.2177±0.0080	0.0232±0.0004	0.1963±0.0080
P4	0.2333±0.0040	0.0222±0.0008	0.2114±0.0027

Table 1: Measures of filling factor across [S IV], [Ne II], and [O IV] in P2 and P4. These values are reflective of the data seen in Figure 3 and Figure 4, where all emission below the standard deviation is assumed to be devoid of the ion.

DeLaney, T., Kossim, N. E., Rothnick, L., & Perley, R. A. 2014, *ApJ*, 785, 7, doi: 10.1088/0004-637X/785/1/7
DeLaney, T., Rothnick, L., Stagg, M. D., et al. 2010, *ApJ*, 725, 2008, doi: 10.1088/0004-637X/725/2/2008
Emswiler, J. A., Rothnick, L., Reich, W. T., et al. 2006, *ApJ*, 652, 376, doi: 10.1086/508142
Gardner, J. P., Mather, J. C., Abbott, R., et al. 2023, arXiv e-prints, arXiv:2304.01860, doi: 10.48550/arXiv:2304.01860
Hines, D. C., Rieke, G. H., Gordon, K. D., et al. 2004, *ApJS*, 154, 291, doi: 10.1086/422583
Hwang, U., & Laming, J. M. 2012, *ApJ*, 746, 130, doi: 10.1088/0004-637X/746/2/130
Isensee, K., Rothnick, L., DeLaney, T., et al. 2010, *ApJ*, 725, 2059, doi: 10.1088/0004-637X/725/2/2059
Laming, J. M., & Temim, T. 2020, *ApJ*, 904, 115, doi: 10.3847/1538-4357/ab1c65
Milisavljević, D., & Fesen, R. A. 2013, *ApJ*, 772, 134, doi: 10.1088/0004-637X/772/2/134
Milisavljević, D., Temim, T., De Looze, I., et al. 2024, *ApJL*, 965, L27, doi: 10.3847/2041-8213/ad347f
Smith, N., Silverman, J. M., Chirokov, R., et al. 2009, *ApJ*, 695, 1331, doi: 10.1088/0004-637X/695/2/1331
This work is based on observations made with the NASA/ESA/CSA James Webb Space Telescope. The data were obtained from the Mikulski Archive for Space Telescopes at the Space Telescope Science Institute, which is operated by the Association of Universities for Research in Astronomy, Inc., under NASA contract NAS 5-03127 for JWST. These observations are associated with program #1947. Support for program #1947 was provided by NASA through a grant from the Space Telescope Science Institute, which is operated by the Association of Universities for Research in Astronomy, Inc., under NASA contract NAS 5-03127. Distribution Statement A. Approved for public release; distribution unlimited.
We acknowledge the invaluable support from Mark Livill and Chris Orr who help manage computational resources used to complete this research. D.M. acknowledges NSF support from grants PHY-2209451 and AST-2206532. T.T. acknowledges support from the NSF grant 2205314 and the JWST grant JWST-GO-01947.031. J.M.L. was supported by JWST grant JWST-GO-01947.023 and by basic research funds of the Office of Naval Research. I.D.L. acknowledges funding from the Belgian Science Policy Office (BELSPO) through the PRODEX project "JWST MIRI Science exploitation" (C400142239). I.D.L. has received funding from the European Research Council (ERC) under the European Union's Horizon 2020 research and innovation programme "DestOrigin" (ERC-2019-SG-851022). B.-C.K. acknowledges support from the Basic Science Research Program through the NRF of Korea funded by the Ministry of Science, ICT and Future Planning. (RS-2024-0027370). Work by B.G.A. was supported by NASA under award number 80SP21M002.